View metadata, citation and similar papers at core.ac.uk

brought to you by CORE

東北大学機関リポジトリ
TOUR
Tohoku University Repository

Submicrometer Comb-Drive Actuators Fabricated on Thin Single Crystalline Silicon Layer

著者	羽根　一博
journal or publication title	IEEE Transactions on Industrial Electronics
volume	56
number	4
page range	991-995
year	2009
URL	http://hdl.handle.net/10097/46526

doi: 10.1109/TIE.2008.2006934

Submicrometer Comb-Drive Actuators Fabricated on Thin Single Crystalline Silicon Layer

Kazunori Takahashi, Erdal Bulgan, Yoshiaki Kanamori, and Kazuhiro Hane

***Abstract*—Electrostatic comb-drive microactuators were fabricated by electron beam lithography on a 260-nm-thick silicon layer of a silicon-on-insulator wafer. The actuators consisted of comb electrodes, springs, and a frame. Two kinds of microactuators with doubly clamped and double-folded springs were designed and fabricated. The comb electrode was as small as 2.5 μm wide and 8 μm long and was composed of 250-nm-wide, 260-nm-thick, and 2-μm-long fingers. The air gap between the fingers was 350 nm. The spring was 250 nm wide, 260 nm thick, and 17.5 μm long, and the spring constant was 0.11 N/m. The force and displacement generated by the microactuator were 2.3×10^{-7} N and 1.0 μm, respectively. Applying an ac voltage, the oscillation amplitude became maximum at a frequency of 132 kHz. The mechanical and electrical characteristics of the fabricated actuators were investigated quantitatively.**

***Index Terms*—Actuators, microelectromechanical devices, micromachining.**

I. Introduction

MICROACTUATORS are key components in microelectromechanical systems (MEMS). In optics, the mirror displacement equal to a wavelength can generate 4π phase shift of lightwave, which is enough to compensate an interferometric phase [1], [2]. A small gap change in a micromachined capacitor generates a wide-range tuning of capacitance at radio frequency [3]. Microactuators are also used in the manipulation of micro-objects such as cells and biological materials [4], [5]. Those tuning and manipulation techniques using microactuators cannot always be replaced by other methods. Therefore, not only in scientific research but also in industry, microactuators are indispensable. The technology of steering lightwave by microactuators has already been used in optical projection displays [6] and optical switches [7].

Among the microactuators proposed in MEMS research, those using electrostatic force between the facing electrodes are the most commonly adopted because of their high energy density and monolithic fabrication based on silicon micromachining. In particular, comb-drive actuators have been investigated intensively for a long time. Sophisticated comb structures were fabricated in order to extend the motion range [8], [9] to decrease the actuation voltage [10] and to improve against the instability by pull-in motion [11]. Special attention was also paid to decreasing the driving voltage using submicrometer gap comb-drive microactuators [12]. A high-aspect-ratio comb fabricated on a silicon-on-insulator (SOI) wafer increased the electrostatic force of comb-drive actuator with extended travel range [13]. High-aspect-ratio structure was also studied for polysilicon MEMS [14]. In addition to the aforementioned improvements in device structures, thermal issues in MEMS actuators and microscale systems were also widely discussed [15]. However, most of the comb-drive actuators reported previously consisted of several-micrometers-wide comb fingers, and the total actuator areas were in the range from 0.1 to 1 mm^2. In recent years, in parallel to the progress of micro/nanofabrication, nanoelectromechanical systems have attracted increasing attention. Nevertheless, there have been few reports on the electrostatic comb-drive actuators having submicrometer structures [16].

In this paper, the electrostatic comb-drive actuators with the dimensions smaller by two orders of magnitude in area than the conventional comb-drive actuators are designed and fabricated by electron beam lithography. The proposed actuators consist of comb electrodes, springs, and a frame, which are fabricated on a 260-nm-thick single crystalline silicon layer. The characteristics of the fabricated devices are investigated quantitatively. Extremely small electrostatic comb actuators proposed in this paper can be useful for such MEMS applications as the silicon photonic crystal devices with variable mechanisms [17], silicon nanowire waveguide devices [18], nanoscale positioning systems [19], etc.

II. Design, Fabrication, and Experimental Setup

Fig. 1(a) shows an electrostatic comb-drive actuator (type-1) combined with the doubly clamped springs. The comb electrode consists of 29 finger pairs. Each finger is 200 nm wide, 260 nm thick, and 1.5 μm long. Air gap between each finger pair is 200 nm. The comb area is 2.85 μm wide and 23.4 μm long. Each of the spring elements is a simple straight silicon bar with a width of 200 nm, a thickness of 260 nm, and a length of 12.15 μm.

The second type of the electrostatic comb-drive actuator (type-2) is shown in Fig. 1(b). Each comb finger is 250 nm wide, 260 nm thick, and 2 μm long. Air gap between each finger pair is 350 nm. The comb area is 2.5 μm wide and 8 μm long. The spring structure of type-2 actuator is different from that of type-1. Instead of the doubly clamped springs, double-folded springs are utilized. Each of the spring elements is a straight silicon bar with a width of 250 nm, a thickness of 260 nm, and a length of 17.5 μm, which corresponds to a spring constant of 0.11 N/m. The equivalent shape of the double-folded spring is

Manuscript received March 29, 2008; revised September 3, 2008. First published October 31, 2008; current version published April 1, 2009. This work was supported by a Grant-in-Aid for Scientific Research, JSPS, Japan.

The authors are with the Department of Nanomechanics, Tohoku University, Sendai 980-8579, Japan (e-mail: hane2@hane.mech.tohoku.ac.jp).

Color versions of one or more of the figures in this paper are available online at http://ieeexplore.ieee.org.

Digital Object Identifier 10.1109/TIE.2008.2006934

0278-0046/$25.00 © 2009 IEEE

Authorized licensed use limited to: TOHOKU UNIVERSITY. Downloaded on March 08,2010 at 02:07:38 EST from IEEE Xplore. Restrictions apply.

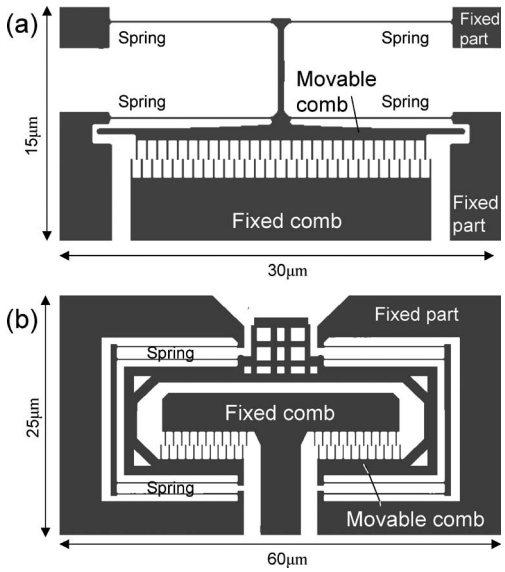

Fig. 1. Design schematics of the electrostatic comb actuators. (a) Type-1 actuator (whole area is 15×30 μm). (b) Type-2 actuator (25×60 μm).

similar to a one-end fixed cantilever. The other end of the spring (the middle point of the double-folded spring) is rotation fixed and translation free.

From the electrostatic model of the comb structure, force generated by comb actuators is given in [9]. On the other hand, the spring constant of a straight silicon bar with one fixed end, and the other end that is rotation fixed and translation free, is given by the following, assuming a small deformation:

$$k = \frac{Ehb^3}{L^3} \tag{1}$$

where E is the young modulus of silicon. The symbols h, b, and L are the spring thickness equal to that of top silicon layer, width of the spring in the bending plane, and length of the spring, respectively. In the case of type-1 actuator, since the movable part is supported by the four springs, the total spring constant k_1 is four times larger than the value of (1). For type-2 actuator, the total spring constant k_2 is twice larger than the value of (1). Using the design sizes of the structures and $E = 1.5 \times 10^{11}$ N/m^2, k_1 and k_2 are calculated to be 0.70 and 0.23 N/m, respectively. In the case of the type-1 actuator spring, the linearity assumption fails after a certain displacement.

The relation between the generated force (or the applied voltage) and the displacement x can be obtained from the balance between the electrostatic force generated by the combs and the reaction force by the spring. The balance equation can be expressed as

$$k_{1,2}x = \varepsilon_0 hN \left(\frac{1}{g} + \frac{w}{(D_0 - x)^2}\right) V^2. \tag{2}$$

Here, the symbol ε_0 is the permittivity of vacuum, N is the number of comb fingers, and V is the applied voltage. The symbols h, g, w, and D_0 denote the thickness of comb equal to that of the top silicon layer, gap between the fingers, width of each finger, and initial distance between top and the bottom of the facing combs, respectively. The theoretical relation between the displacement and the applied voltage is obtained from (2).

Scaling law [20] states that the displacement of the actuator increases linearly at the same voltage if the size of the actuator decreases in all dimensions with the same ratio. The response time of the actuator, which is the time needed for settling the motion after a step voltage is applied, shortens linearly with the decrease in size.

In the fabrication of the designed actuators, electron beam lithography was utilized. An SOI wafer with a 260-nm-thick top silicon layer and a 2.0-μm SiO_2 layer was used. The top silicon layer was used for the actuators, and the SiO_2 layer was etched sacrificially to release the actuator. After cleaning, the wafer was coated with a 350-nm-thick positive polymer resist (ZEON Co., Ltd., ZEP-520A). The spin-coated resist was exposed to electron beam at a dose of around 80 μC/cm^2. The optimum dose for the pattern generation was dependent on the smallest feature width. For example, the optimum dose for a comb pattern was different from the one for a contact electrode pattern. The doses for the respective parts of the microactuators were adjusted to obtain their optimum conditions. After the development of the resist, top silicon layer was etched by fast atom beam, which was generated by the neutralization of the ions extracted from a dc SF_6 plasma (Ebara Company, Ltd., FAB-60ML). The etching ratio between the polymer resist and silicon layer was 0.73 at an etching rate of 16 nm/min. Finally, the hydrofluoric acid vapor generated by heating hydrofluoric acid solution was used to etch the SiO_2 layer underneath the etched top silicon layer [21]. The movable part suspended by narrow silicon springs was easily stuck by capillary forces if the sacrificial SiO_2 layer was removed by the hydrofluoric acid solution. Due to the hydrofluoric acid vapor, the fine movable part can be released without the stiction problem.

The displacement of the actuator is measured from the micrograph obtained in the scanning electron microscope (SEM). Since the size of the movable part of the device is small, it is difficult to observe clearly by conventional optical microscopy. In the case of out-of-plane displacement, optical interferometric probe is a powerful tool. On the contrary, in the case of in-plane motion, a high resolution imaging system is needed. SEM has a high lateral resolution. However, since SEM images are obtained by raster scanning, the time for image acquisition is long. The displacement of the actuator under dc operation was obtained after magnification calibration. On the other hand, in the case of oscillation at the frequencies higher than the raster scan frequency, a time-averaged SEM image is obtained. The SEM system utilized in this paper for displacement and vibration amplitude measurement is shown in Fig. 2. High voltages can be applied from the outside of SEM chamber to the device in vacuum. If an edge part of the sample oscillating at a frequency much higher than the raster scan frequency is imaged, a time-averaged image of the edge is obtained. From the width of the edge image, the oscillation amplitude can be measured. Thus, the phase information of the oscillation gets lost.

III. Results and Discussion

Fig. 3(a) and (b) shows the scanning electron micrographs of the fabricated actuators of type-1 and type-2, respectively, which were obtained under the conditions that the actuation

Authorized licensed use limited to: TOHOKU UNIVERSITY. Downloaded on March 08,2010 at 02:07:38 EST from IEEE Xplore. Restrictions apply.

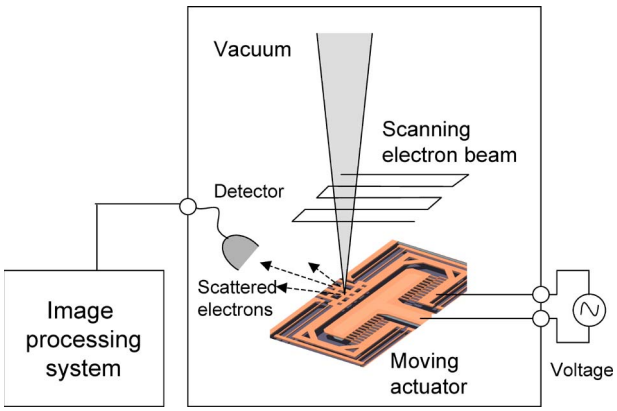

Fig. 2. SEM measurement system for displacement and oscillation amplitude.

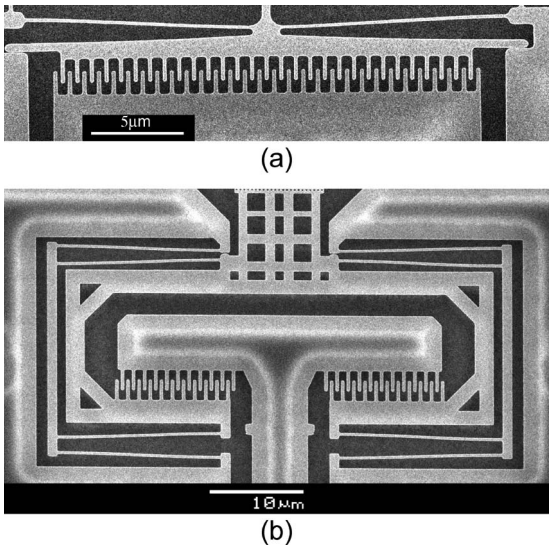

Fig. 3. Scanning electron micrographs. (a) Type-1 actuator at an applied voltage of 65 V. (b) Type-2 actuator at 22 V.

voltages of 65 V (around 540-nm displacement) and 22 V (around 1-μm displacement) were applied to the comb electrodes, respectively. As shown in Fig. 3(a) and (b), the comb-drive actuators with the submicrometer combs were fabricated properly. The comb fingers are 185 $\pm$ 20 nm wide in Fig. 3(a) and 315 $\pm$ 30 nm wide in Fig. 3(b), evaluated from the SEM images. The long narrow springs with the widths of 190 nm for type-1 and 310 nm for type-2 were properly fabricated as well.

After etching the sacrificial layer by hydrofluoric acid, released structures were examined under an optical surface profiler. The movable comb and the springs of the type-1 actuator were sometimes lifted or shifted laterally by thermal stress released in the top silicon layer. The magnitude and direction of the bonding stress in SOI wafers are dependent on the fabrication process [22]. The stress was compressible in our wafer before sacrificial layer etching. In the case of type-1 actuator, the movable part was suspended by the four springs. The etched structure was lifted by the release of the thermal stress. After the release, the top silicon layer had very little stress if the structure was freely supported. However, a bending moment was generated around the fixed position of the beam, as discussed in [23]. Therefore, the top silicon layer

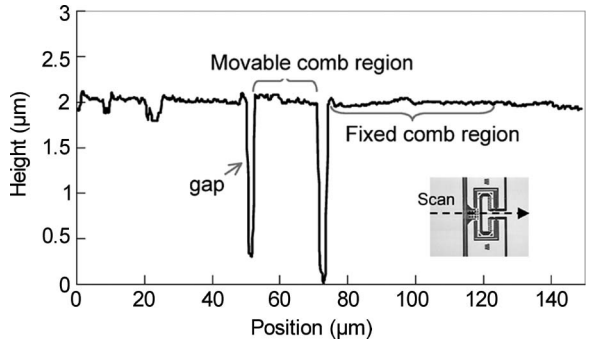

Fig. 4. Surface profile of the fabricated actuator (type-2) measured as a function of position.

was lifted vertically away from the substrate, which caused a height difference between the movable part and the fixed parts. The deflected structure caused a deviation in actuation characteristics with respect to the theoretical design.

In order to prevent the influence of the stress release, the type-2 actuator was designed and fabricated. In the type-2 actuator, springs were connected to make a U-shaped spring. Therefore, both ends of the springs were fixed to a side of the silicon substrate. Therefore, unlike type-1 actuator, the movable part was not lifted. The surface of the fabricated type-2 actuator was scanned with a laser beam of optical surface profiler to obtain the height distribution along a scan line. An example of the scanning results is shown in Fig. 4. The maximum height difference is smaller than 50 nm, as shown in Fig. 4. In the case of type-1 actuator, the height difference was sometimes larger than 700 nm for the structure mechanically equivalent to type-2 actuator.

The mechanical characteristics of the fabricated actuators were investigated. The displacement of the actuators was measured as a function of the applied voltage. Fig. 5(a) and (b) shows the displacements of type-1 and type-2 actuators, respectively, as a function of the applied voltage. In the case of type-1 actuator, the displacement increases gradually with the increase of the voltage. The displacement of 460 nm is obtained at a voltage of 45 V, as shown in Fig. 5(a). The calculated displacement is also shown in Fig. 5(a), which can explain roughly the experimental values at lower voltages. Theoretical calculations were carried out using actuator design values. At large voltage, the experimental value of the displacement is smaller than the calculated value, which is considered to be caused by the levitation described in the surface profile measurements. The levitation decreases the generated electrostatic force since the overlapping area becomes smaller than the design value.

In the case of type-2 actuator, measured displacement also increases quadratically as a function of the applied voltage, as shown in Fig. 5(b). At a voltage of 22 V, a displacement of 1 μm is obtained. The relative variation and the absolute value of the displacement are well explained by the theoretical calculations.

Many continuous systems, such as doubly clamped beams, have cubic nonlinearities arising from midplane stretching. Dynamic macromodels for electrically actuated MEMS devices were studied and were successful for explaining the effects of nonlinearities on the system behavior [24]. According to the linear theory, resonance occurs when the driving frequency is

Authorized licensed use limited to: TOHOKU UNIVERSITY. Downloaded on March 08,2010 at 02:07:38 EST from IEEE Xplore. Restrictions apply.

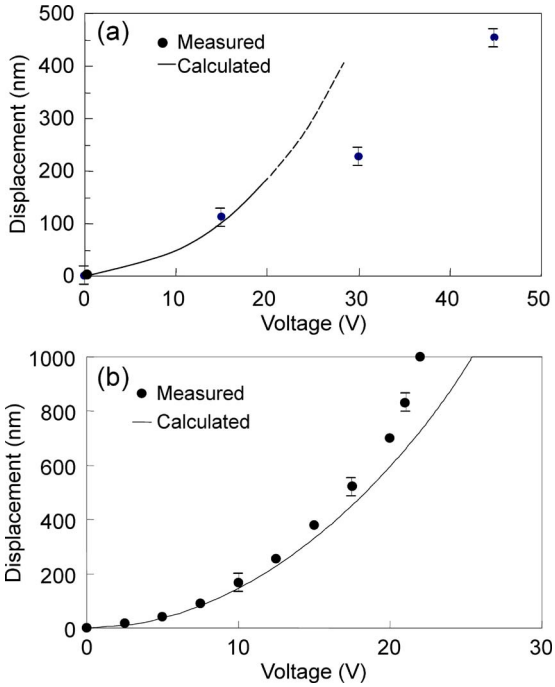

Fig. 5. Calculated and measured displacements as a function of applied voltages. (a) Type-1 actuator. (b) Type-2 actuator.

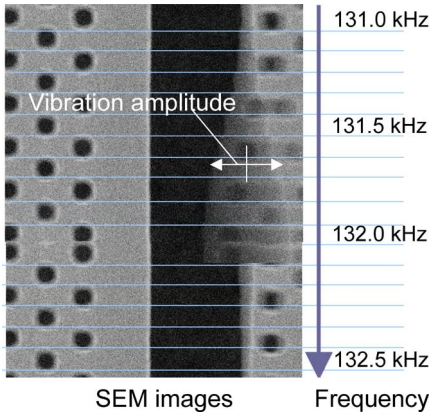

Fig. 6. Time-averaged SEM images of the vibrating actuator edge arrayed with the excitation frequency.

close to the natural frequency. This case corresponds to primary or main resonance. The amplitude in response to any harmonic excitation is determined by the usual peaked resonance curve. However, for a system with Duffing nonlinearity, the frequency response curve of the amplitude is bent to the right- or left-hand side, depending on the nonlinearity. Such a bend in the frequency response curve leads to multiple equilibrium states at several frequencies and, hence, to jump phenomena. The state depends on the initial conditions and the time dependence of the driving function. Jump in amplitudes occurs if the system changes its equilibrium state from one position to another one at the same frequency.

The oscillation amplitude of the type-2 actuator was measured in SEM. Due to the deformation, the properties of type-1 actuator were not always stable. Therefore, type-2 actuator was investigated in detail. Fig. 6 shows the electron micrograph of the oscillating part of the actuator, which depicts the response

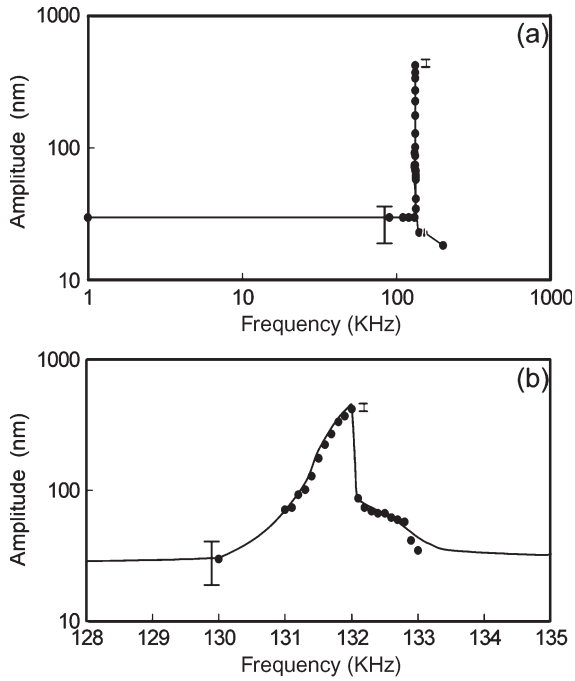

Fig. 7. Oscillation amplitude measured as a function of the frequency of the applied voltage for the type-2 actuator.

to the driving frequencies. The figure is a composite of bands of images of the same section of the device under various frequency loading conditions. With the increase of the frequency from 131 kHz, the oscillation amplitude increases since the oscillating edge of the time-averaged image is expanded. The amplitude reaches to a peak value at 132.05 kHz, and then, the amplitude suddenly decreases, as can be seen in Fig. 6.

The vibration amplitude of the type-2 actuator is shown in logarithmic scale in Fig. 7(a) as a function of the frequency in the range from 1 Hz to 200 kHz at an ac voltage of 1.1 V. The amplitude is also shown in a narrow frequency region from 128 to 135 kHz around the maximum amplitude in Fig. 7(a). At 132.1 kHz, the maximum amplitude jumps to a lower value. The frequency response curve of the amplitude is seen to be bent to the right-hand side [24].

The natural frequency can be estimated theoretically from a linearized spring-mass model. The spring constant for the type-2 actuator is calculated from the dimensions, the elastic constant of silicon, which is 0.23 N/m, and the mass, which is 2.3×10^{-13} kg. The natural frequency given by $f_0=(\sqrt{k/m})/(2\pi)$ is equal to 158 kHz, which can explain the measured value roughly. The response time of the type-2 actuator may be evaluated from the inverse of the natural frequency, which is around 8 μs. Therefore, the responses of the studied microactuators are much faster than those of the conventional ones.

IV. Conclusion

Electrostatic comb microactuators having an area smaller by two orders of magnitude than the conventional microactuators were fabricated by electron beam lithography on an SOI wafer with a 260-nm-thick top silicon layer. Two types of microactuators were designed, fabricated, and tested. Due to the thermal stress release of the SOI wafer, a considerable distortion was

Authorized licensed use limited to: TOHOKU UNIVERSITY. Downloaded on March 08,2010 at 02:07:38 EST from IEEE Xplore. Restrictions apply.

observed in the movable part of the type-1 actuator. Although the released part of the actuator was nearly free from the stress, the stress of the SOI wafer generated a bending deformation at the borders of the fixed position of the springs. In the type-2 actuator, the spring structure was modified not to be affected by the stress release. A displacement of 1 μm was obtained at a voltage of 22 V, and the maximum oscillation amplitude was obtained at a frequency of 132 kHz. The obtained results were consistent with the scaling law. By decreasing the size of the actuators, the fabricated actuators responded much faster than those of conventional size.

REFERENCES

[1] Y. Uenishi, K. Honma, and S. Nagaoka, "Tunable laser diode using a nickel micromachined external mirror," *Electron. Lett.*, vol. 32, no. 13, pp. 1207–1208, Jun. 1996.

[2] A. Spisser, R. Ledantec, C. Seassal, J. L. Leclercq, T. Benyattoou, D. Rondi, R. Blondeau, G. Guillot, and P. Viktorovitch, "Highly selective and widely tunable 1.55-μm InP/air-gap micromachined Fabry–Perot filter for optical communications," *IEEE Photon. Technol. Lett.*, vol. 10, no. 9, pp. 1259–1261, Sep. 1998.

[3] D. M. Klymyshyn, D. T. Haluzan, M. Borner, S. Achenbach, J. Mohr, and T. Mappes, "High aspect ratio vertical cantilever RF-MEMS variable capacitor," *IEEE Microw. Wireless Compon. Lett.*, vol. 17, no. 2, pp. 127–129, Feb. 2007.

[4] M. Sato, K. Nagayama, N. Kataoka, M. Sasaki, and K. Hane, "Local mechanical properties measured by atomic force microscopy for cultured bovine endothelial cells exposed to shear stress," *J. Biomech.*, vol. 33, no. 1, pp. 127–135, Jan. 2000.

[5] J. Krayer, S. Tatic-Lucic, and S. Neti, "Micro-arheometer: High throughput system for measuring of viscoelastic properties of single biological cells," *Sens. Actuators B, Chem.*, vol. 118, no. 1/2, pp. 20–27, Oct. 2006.

[6] L. J. Hornbeck, "Projection displays and MEMS: Timely convergence for a bright future," in *Proc. SPIE Conf.*, 1995, vol. 2639, p. 2.

[7] P. M. Dobbelaere, S. Gloeckner, S. K. Patra, L. Fan, C. King, and K. Faita, "Design, manufacture and reliability of 2-D MEMS optical switches," in *Proc. SPIE Conf.*, 2003, vol. 4945, pp. 39–45.

[8] M. Wu, H. Lin, R. Chen, and W. Fang, "A novel sequential engagement electrodes for vertical comb-drive actuator," in *Proc. MEMS*, 2007, pp. 655–658.

[9] G. Zhou and P. Dowd, "Tilted folded-beam suspension for extending the stable travel range of comb-drive actuators," *J. Micromech. Microeng.*, vol. 13, no. 2, pp. 178–183, Mar. 2003.

[10] M. Sasaki, S. Yuki, and K. Hane, "Large-rotation and low-voltage driving of micromirror realized by tense thin-film torsion bar," *IEEE Photon. Technol. Lett.*, vol. 18, no. 15, pp. 1573–1575, Aug. 2006.

[11] J. D. Grade, H. Jerman, and T. W. Kenny, "Design of large deflection electrostatic actuators," *J. Microelectromech. Syst.*, vol. 12, no. 3, pp. 335–343, Jun. 2003.

[12] T. Hirano, T. Furuhata, K. J. Gabriel, and H. Fujita, "Design, fabrication, and operation of submicron gap comb-drive microactuators," *J. Microelectromech. Syst.*, vol. 1, no. 1, pp. 52–59, Mar. 1992.

[13] Y. Sun, D. Piyabongkarn, A. Sezen, B. J. Nelson, and R. Rajamani, "A high-aspect-ratio two-axis electrostatic microactuator with extended travel range," *Sens. Actuators A, Phys.*, vol. 102, no. 1/2, pp. 49–60, Dec. 2002.

[14] F. Ayazi and K. Najafi, "High aspect-ratio dry-release poly-silicon MEMS technology for inertial-grade microgyroscopes," in *Proc. IEEE Position Location Navigat. Symp.*, San Diego, CA, 2000, pp. 304–308.

[15] D. L. De Voe, "Thermal issues in MEMS and microscale systems," *IEEE Trans. Compon. Packag. Technol.*, vol. 25, no. 4, pp. 576–583, Dec. 2003.

[16] E. Bulgan, Y. Kanamori, and K. Hane, "Submicron silicon waveguide optical switch driven by microelectromechanical actuator," *Appl. Phys. Lett.*, vol. 42, no. 10, pp. 101 110-1–101 110-3, Mar. 2008.

[17] K. Umemori, Y. Kanamori, and K. Hane, "Photonic crystal waveguide switch with a microelectromechanical actuator," *Appl. Phys. Lett.*, vol. 89, no. 2, pp. 021 102-1–021 102-3, Jul. 2006.

[18] H. Yamada, T. Chu, S. Ishida, and Y. Arakawa, "Si photonic wire waveguide devices," *IEEE J. Sel. Topics Quantum Electron.*, vol. 12, no. 6, pp. 1371–1379, Nov./Dec. 2006.

[19] M. Esashi and T. Ono, "From MEMS to nanomachine," *J. Phys. D, Appl. Phys.*, vol. 38, no. 13, pp. R223–R230, Jul. 2005.

[20] W. S. N. Trimmer, "Microrobots and micromechanical systems," *Sens. Actuators*, vol. 19, no. 3, pp. 267–287, Sep. 1989.

[21] Y. Fukuta, H. Fujita, and H. Toshiyosi, "Vapor hydrofluoric acid sacrificial release technique for micro electro mechanical systems using labware," *Jpn. J. Appl. Phys.*, vol. 42, no. 6A, pp. 3690–3694, Jun. 2003.

[22] F. M. Kamm, A. Ehrmann, H. Schafer, W. Pamler, R. Kasmaier, J. Butschke, R. Springer, E. Haugeneder, and H. Loschner, "Influence of silicon on insulator wafer stress properties on placement accuracy of stencil masks," *Jpn. J. Appl. Phys.*, vol. 41, no. 6B, pp. 4146–4149, Jun. 2002.

[23] W. Feng and J. A. Wickert, "Determining mean and gradient residual stresses in thin films using micromachined cantilevers," *J. Micromech. Microeng.*, vol. 6, no. 3, pp. 301–309, Sep. 1996.

[24] J. E. Mehner, L. D. Gabbay, and S. D. Senturia, "Computer-aided generation of nonlinear reduced-order dynamic macromodels. II: Stress-stiffened case," *J. Microelectromech. Syst.*, vol. 9, no. 2, pp. 270–278, Jun. 2000.

Kazunori Takahashi received the B.S. and M.S. degrees in mechanical engineering from Tohoku University, Sendai, Japan, in 2006 and 2008, respectively.

He is currently a Researcher with Shimadzu Corporation, Kyoto, Japan.

Erdal Bulgan received the M.S. degree in manufacturing systems engineering from the University of Wisconsin, Madison, in 1999. He is currently working toward the Ph.D. degree in the Department of Nanomechanics, Tohoku University, Sendai, Japan.

From 2001 to 2005, he was a Lecturer with the Department of Mechanical Engineering, Izmir Institute of Technology, Izmir, Turkey. He is currently involved in the study and development of silicon photonic devices utilizing MEMS technology.

Yoshiaki Kanamori received the M.S. and Dr. Eng. degrees from Tohoku University, Sendai, Japan, in 1998 and 2001, respectively.

From 1998 to 2001, he was a Research Fellow with the Japan Society for the Promotion of Science. From 2001 to 2007, he was a Research Associate with the Graduate School of Engineering, Tohoku University. From 2003 to 2004, he was a Postdoctoral Researcher with the Laboratory for Photonics and Nanostructures Center, Centre National de la Recherche Scientifique, Paris, France. Since 2007, he has been an Associate Professor with the Department of Nanomechanics, Tohoku University. He is currently engaged in research and development of optical microsensors and optical MEMS.

Kazuhiro Hane received the M.S. and Dr. Eng. degrees from Nagoya University, Nagoya, Japan, in 1980 and in 1983, respectively.

From 1983 to 1994, he was a member of the faculty of the Department of Electrical Engineering, Nagoya University. From 1985 to 1986, he was a Visiting Researcher of the National Research Council of Canada. Since 1994, he has been a Professor with the Department of Nanomechanics, Tohoku University, Sendai, Japan, where he is currently engaged in research and development of optical microsensors and optical MEMS.

Authorized licensed use limited to: TOHOKU UNIVERSITY. Downloaded on March 08,2010 at 02:07:38 EST from IEEE Xplore. Restrictions apply.